Microstructural hwestigation of SDM Microcasting Droplets

CM. Bishop, SA Spencer, K.S. Schmaltz, and CH. Amon

EDRC 24-127-97

Microstructurai Investigation of SDM Microcasting Droplets

CM. Bishop, S.A. Spencer, K.S. Schmaltz and C.H. Amon
EDRC Technical Report 24-127-97,
Carnegie Mellon University, Pittsburgh, PA

This work has been supported by the Engineering Design Research Center,
a NSF Engineering Research Center.

Abstract:

Our research efforts seek to improve the fundamental understanding of the deformation and solidification of metal droplets, which is applicable to Shape Deposition Manufacturing (SDM) Microcasting. Research includes direct numerical simulations of the process and a variety of experimental techniques to validate the numerical models. This report details our use of microstructural characterization as a validation technique. Individual microcasting droplets are cross-sectioned, etched and examined by optical microscope. Energy dispersive x-ray analysis (EDX) is also used to identify material composition in samples that involve dissimilar materials. Using these techniques we are able to gain a qualitative understanding of the cooling process through variations in microstructure, and quantitative estimates of both cooling rates (through dendrite arm spacing measurements) and substrate remelting (through structure change in the substrate). This information is being compared with numerical results to confirm the accuracy of our numerical models.

Introduction:

We are investigating the microstructure of metal deposition via Shape Deposition Manufacturing (SDM) Microcasting in an effort to understand the physical processes and to validate our numerical modeling. SDM is a solid freeform fabrication approach being developed to directly create functional metal structures (Merz, 1994). These structures can be arbitrarily complex and three-dimensional, generated directly from CAD models, and made without part-specific tooling or human intervention. Final artifacts are fully dense, have controlled microstructures and acceptable surface appearance, and are within specified dimensional tolerances. SDM microcasting parts are incrementally built-up using a combination of material deposition and removal processes shown in Figure 1. Individual layer segments are deposited as near-net shapes and then accurately machined to net-shape before depositing additional material. Each layer consists of both primary material (308 stainless steel) and sacrificial material (copper) which is removed after the part has been completely built up.

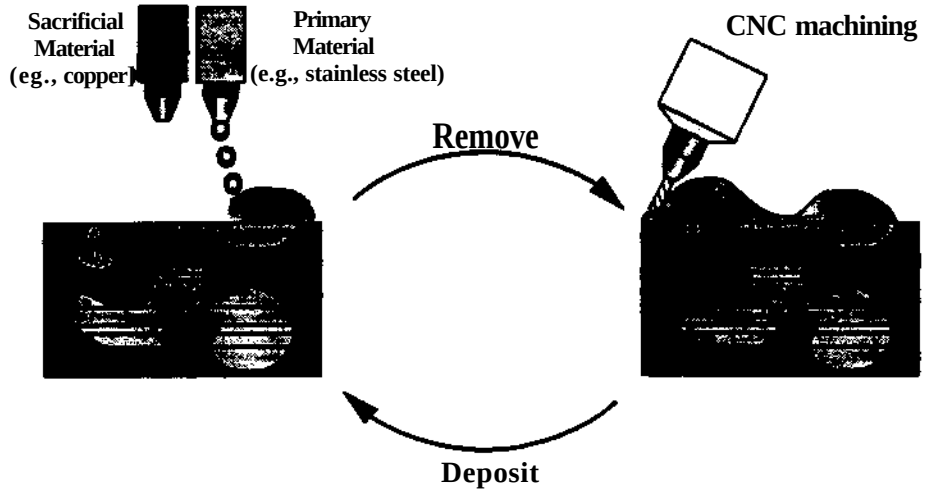

Figure 1. Shape Deposition Manufacturing

During microcasting, an arc is established between a conventional plasma welding torch and feedstock wire which is supplied from a charged contact tip. Deposition material melts in the arc and falls as droplets from the wire; accelerated by gravity, the droplets flatten upon impact with the substrate. In contrast to the micron-sized droplets created with thermal spraying, the diameters of microcast droplets are on the order of millimeters. The droplets fall several inches, through an inert, nitrogen environment, and strike the substrate with a velocity on the order of one meter per second.

The plasma torch generates microcast droplets with a significant amount of superheat. Due to the large volume-to-surface ratio, the droplets remain superheated in flight and contain sufficient energy (temperatures at impact in excess of 2,000°C) to locally remelt the underlying substrate at impact to form metallurgical bonding upon solidification. While an entire droplet solidifies in an order of tenths of a second, the substrate remelting and resolidification process concludes over an order of magnitude faster. This remelting phenomenon is a critical aspect of SDM microcasting because the final quality of a part created by the process is dependent on achieving this type of bonding. Part strength and material properties are comparable to traditionally formed parts when remelting has been achieved, but will be greatly reduced if the part is a series of weakly bonded layers.

A combination of experimental and numerical efforts are underway to understand and improve the SDM process. Deposition experiments investigate the relation between microcasting process parameters (e.g., plasma current, wirefeed rate, droplet standoff) and droplet characteristics (Osio 1996; Padmanabhan, 1996), and the influence of application parameters on the resulting deposited artifact quality, measured as the volume percentage of voids present in a deposited layer (Osio and Amon, 1996; Osio et al., 1997). The numerical simulations predict the interface heat transfer at droplet impact, the spreading behavior of the solidifying droplet, and the overall cooling of both individual droplets and successive layers (Amon et al., 1996a). Experiments also provide the process conditions needed for numerical studies, such as the size, temperature and velocity of the droplet striking the substrate, while the numerical simulations yield the amount of partial substrate remelting, and cooling history. An accurate understanding of the thermal history is also important to predict and mitigate the effects of thermally induced stresses (Amon et al., 1996b).

The motivation behind our research is to understand and control the SDM interface remelting phenomenon. High quality bonds between layers are sought for the strength and integrity of the final artifact created. Excessive heat and remelting are to be avoided to reduce the accumulated residual stresses generated, and to preserve the quality of the exterior surface of the artifacts (for the copper/stainless steel interface). Achieving these goals requires an accurate understanding of the heat transfer taking place during droplet solidification. Performing a microstructural characterization of the droplets and the interface between droplet and substrate provides a useful tool in validating the accuracy of our numerical models, and in gaining a qualitative knowledge of the bonding phenomenon. For the study reported here, the microstructures of each of the four combinations of droplet and substrate materials are considered. Droplets are generated over the range of plasma

power available with SDM microcasting, for each combination of droplet/substrate material. A more detailed investigation of the microstructure is performed for the upper and lower values of the plasma power level range; the microstructure for each of these eight cases (four material combinations, two power levels) is determined over a spatially systematic pattern, within the droplet region and the substrate region. Lower magnification (SOX or 100X) views provide a qualitative understanding of the interface remelting and bonding, while higher magnification (500X or 1000X) views yield dendrite arm spacing information needed to estimate cooling rates.

Microstructure Theory:

We are using microstructural characterization as an experimental tool to improve our understanding of the microcasting process. Through the direct examination of sample droplets deposited, and by comparison of experimental cooling rate estimates with results from the numerical simulations, these experiments help to validate our predictive tools, and offer qualitative and quantitative information regarding the microcasting process.

The dendritic solidification is one of the most common structures found in the casting of alloys (Kurz and Fisher, 1992). This structure arises from the combined effects of perturbations at the solid/liquid interface during solidification, together with unequal accumulation of excess solute in the liquid regions ahead of the advancing solidification interface. The concentration of solute increases within the liquid ahead of the growth front due to the lower solubility within the expanding solid region. As crystal growth proceeds, solid phase diffusion is insufficient to keep excess solute from accumulating in the liquid region. The solute concentrations present in the liquid affect the ongoing crystal growth rates (solidification). In alloys, growth rates are controlled by both solute diffusion and heat removal, while in pure materials heat flow controls the growth rates.

With uneven solute accumulation, the interface to become unstable and form cells rather than a smooth interface. This columnar cell growth yields structures called dendrites that are directionaily oriented in the direction of heat flow, and whose growth rate is constrained by the removal of energy by conduction. The microstructure of SDM microcast droplets are observed to be columnar, particularly near the interface of the substrate. An equiaxed microstructure is also seen in the droplets, closer to the top surface. Equiaxed structures, which appear broadly similar to columnar but lack any preferential orientation towards the heat-flow direction, arise from several conditions. The accumulation of solute in the liquid

region alters the alloy liquidus temperature, and for a sufficiently small temperature gradient the liquid region can become undercooled (constitutional undercooling). This creates the conditions necessary for multiple nucleation of crystals to occur. Grain multiplication is another mechanism for the formation of equiaxed structures, caused by the remelting of columnar dendrites, and the bulk convection of dendrite arms. These dendrite grains then become the nucleation sites for equiaxed growth.

The presence of columnar dendrite formations improves our efforts to determine cooling rates from the microstructure. The more regular nature of this structure and the ability to measure the differences in spacing at varied locations add to the quantitative accuracy of our work. Theoretical and experimental relationships are available between dendrite arm spacing and cooling rate. The typical equations for primary and secondary spacing (A_1 and λ_2) are of the form:

$$X_1 = CG^m V^n \tag{1}$$

$$X_2 = K(GV)^m = KR^{ra} \tag{2}$$

where C, K, m and n are empirical constants for a given material; G is the temperature gradient; V is the interface velocity; and R, the product of GV, is the effective cooling rate. This provides us with the ability to estimate the cooling rate by physically measuring the dendrite arm spacing. For our microstructural characterization of the copper we use the cooling rate correlation for primary dendrite arm spacing (with m=n):

$$\lambda_t = 306 \cdot R^{-0.36} \tag{3}$$

The use of secondary dendrite arm spacing is preferred for relating microstructure to thermal history, however with the nearly pure copper material used it is not possible to consistently find secondary dendrites. For stainless steel cooling rates, we use secondary dendrite arm spacing given by:

$$X_2 = 64 \cdot R^{-0.35} \tag{4}$$

For both correlations the dendrite arm spacing, A_1 is measured in microns. R is measured in degrees K per minute for copper (Mills, 1985), and in degrees K per second for the stainless steel (Wolf, 1986).

The accuracy of relating cooling rates to microstructure requires that the experiments be performed under carefully controlled solidification conditions. Slower cooling rates correspond to wider spaced dendrites that can be measured more precisely. The microcasting process is not a carefully controlled process, and the high solidification rates (R) experienced during the microcasting process result in small values for dendrite spacings (K_x and X_2). Correlations for stainless steel between dendrite spacing and cooling rate are available in the literature at these high cooling rates, however, the copper spacing correlation is extrapolated from slower cooling rates (and larger X values). These factors combine to introduce uncertainty or error into our calculations of copper cooling rates that must be accounted for when drawing conclusions about the results.

The second use of microstructural characterization is to verify the occurrence of substrate remelting and quantify (where possible) its extent. For the two cases with similar droplet and substrate materials (steel on steel; copper on copper) the remelting phenomenon leaves a discernible line along the interface, and the original substrate is evident at the edge of the droplet (see Figure 4). Solute accumulation causes a visible line at the deepest penetration of remelting, and the continuity of dendrite structure across this line confirms this location as the edge of the remelt region. For the two cases of dissimilar droplet and substrate materials (steel on copper; copper on steel) the delineation of remelting is less clear. When remelting does occur, there is some mixing of the two materials. By identifying foreign material within a region (i.e. copper within the original stainless steel droplet) we have been able to confirm remelting for these dissimilar material cases. This identification has been performed using scanning electron microscopy to obtain microstructural information. Energy dispersive X-ray analysis (EDX) can characterize the precipitates (small region of material) which are commonly observed in the overall droplet matrix, and thus distinguish copper from stainless steel.

Experimental Procedure

The droplet samples we use for microstructural characterization were available from previous experiments performed to investigate the influence of SDM process application parameters, and to relate the process effect on the droplets to the resulting deposited artifact quality (Osio et al., 1997). Because these droplets were formed over the entire range of parameters possible, samples are available for many different application conditions. We

chose samples from each of the four combinations of materials: stainless steel droplets on stainless steel or copper substrates; and copper droplets on stainless steel or copper substrates. The droplet temperature at impact, the input condition most readily altered by changing application parameters, is determined by the plasma power setting. Prior calorimetry experiments have been performed to correlate the impact temperature of the droplets to the plasma power settings (Merz, 1994). The stainless steel droplet temperature range was 2,000°C to 2,500°C; the copper droplet range was l,800°C to 2,000°C.

The stainless steel droplets are formed from a standard 308 grade welding wire (McKay ER308). The composition is 68% Fe, 20% Cr, 10% Ni, 2% Mn, and trace percentages of Si and C. The solidus temperature at this composition is l,420°C. The copper droplets are formed from de-oxidized copper wire (Natweld DEOX CU), which is 98% Cu, 1% Sn and lesser percentages of Mn, Si, and P. The melting point is approximately l,080°C.

Using the sample plates from previous experiments, droplet samples were sectioned approximately through the droplet centeriine with a band saw. The samples were mounted using Lecoset™ 7007 Cold Curing Resin powder and liquid in a 2:1 volume ratio, and polished using successively finer LECO SiC grit papers (100,240, 320,400, and 600 grit) on rotary polishing wheels. The wheel was set to rotate at about 500 rpm and a steady stream of water was run onto the center of the wheel during polishing to keep the samples cool (avoiding hot-working microstructure changes) and to rinse away the grinding material. The samples were rotated 90° between each paper. Final sample polishing was performed with successively finer alumina slurries of 1.0 |im, 0.3 |im, and 0.05 *im* alumina powders in water (Linde C, A, and B solutions) on LECO Imperial Polishing cloths. A fresh cloth was used for each solution and the samples were rotated 90° between each cloth. Polishing quality was monitored by examination under an optical microscope.

The preferred etchant for stainless steel was found to be Marble's Reagent: 4 g $CuSO_4$, 20 ml H_2O, and 20 ml HC1. The droplet samples were emersed and agitated in the etchant for 15 to 20 seconds then held under running warm water for 15 seconds, cleaned with methanol and dried with warm air. The copper samples were etched with 25 ml NH_4OH, 25 ml H_2O_2 (3%) and 25 ml H_2O (the peroxide added last). These samples were swabbed with the etchant for 5 to 10 seconds then held under running warm water for 15 seconds. Methanol was again used to remove any debris from the samples, followed by warm air drying. With the dissimilar material samples, it was not possible to simultaneously etch

both the stainless steel and the copper regions, since the etchant for stainless steel would excessively etch the copper or cause the copper to bleed across to the stainless steel. Therefore, the microstructures of all samples involving both copper and stainless steel were investigated alternately.

Dendrite arm spacing is determined for both stainless steel and copper droplet samples, deposited on stainless steel or copper substrates, over a wide range of plasma power settings. Dendrite arm spacing is then measured in a systematic fashion at seven droplet locations for eight different samples (each of the four combinations of droplet/substrate materials; and high/low plasma power settings). Figure 2 shows the droplet measurement locations (numbered 1 through 7) along the centerline axis of the droplet, and radially outward from the centerline to the edge of the droplet. Arm spacing measurements for three substrate locations extending radially from the droplet centerline to the droplet edge are also determined.

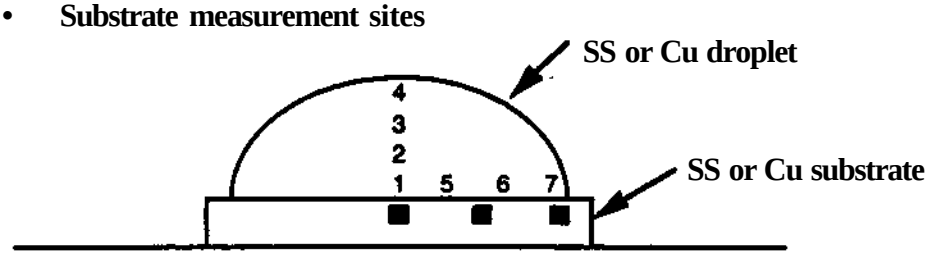

Figure 2. Dendrite Arm Spacing Locations

Optical microscopy of the samples is performed using a LECO® Olympus PME 3 Metallograph at 50X, 100X, 200X, 500X and 1000X magnifications. The lower magnifications (50X, 100X) characterize the rcmelting effect, while the higher magnifications (500X, 1000X) are used to determine the dendrite arm spacing values. Photomicrographs are taken at various magnifications using Polaroid 667 ISO 300 black and white film. A green light filter is used to enhance contrast for the photomicrographs. Dendrite spacing is directly measured from the Polaroid photos, using a superimposed scale as a measurement aid. Spacing measurement accuracy is improved by taking an average across ten dendrites, although it was not always possible to find ten consecutive dendrites to span when the dendrite plane is not closely aligned with the etched surface.

Figure 3 shows representative results of dendrite arm spacing identification. The stainless steel image (Figure 3a on left) is taken at a magnification of 1000X, with the scale

representing 10 *im*. The copper image (Figure 3b on right) magnification is 500X, so the scale represents 20 |xm. For the stainless steel, an average secondary dendrite spacing is determined by measuring the average spacing across 10 secondary arms. For the copper droplet, primary dendrite arm spacing is used for cooling rate calculations. It was not always possible to find regions with a sufficiently regular dendrite pattern to take the average of 10 dendrite arms, and for those cases fewer dendrites are averaged.

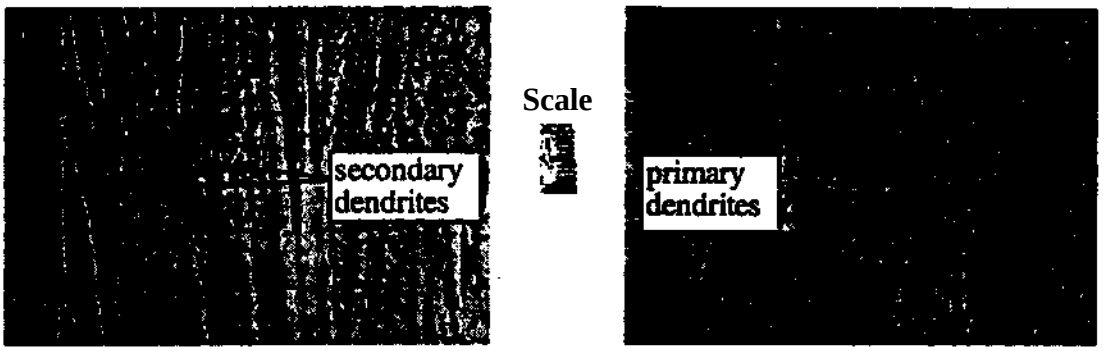

Figure 3. (a) 1000X magnification of stainless steel, (b) 500X magnification of copper.

Samples involving combinations of both stainless steel and copper materials are relevant for the deposition of sacrificial support material. At the interface remelt zone, it is necessary to verify the material present because the microstructural characterization indicates that mixing takes place. The identification of sample material is performed by EDX, using a Princeton Gamma Tech System IV, CamScan Scanning Electron Microscope. The region is identified with this technique at a magnification of 400X, and the corresponding frequency spectrum output (see Figure 8) is used to identify the particular material present. For our dissimilar material cases, we found copper material present within the stainless steel droplets, and stainless steel present within the copper droplets. This confirms the remelting of the substrate by the impinging droplets.

Results:

The results for the first evaluation of dendrite arm spacing within the droplets are shown in Table 1. Twenty-six droplet samples are characterized, with each row in the table representing a different sample. The stainless steel droplets are presented first, and the

copper second. The columns in the table indicate the type of substrate material, the plasma current setting, the measured dendrite spacing (secondary for stainless steel, primary for copper), and the calculated cooling rate (from equation (4) for stainless steel, and equation (3) for copper).

Table 1. Dendrite Arm Spacing Results within Droplets

Steel Droplets Substrate	Current (A)	**Second. Dendrite Arm** Spacing A2(in |xm)	**Calculated Cooling Rate** (°C/sec.)
SS	**84**	**3.6**	**3,700**
SS	**84**	**3.1**	**5,700**
SS	**70**	**2.9**	**6,900**
SS	**70**	**3.2**	**5,200**
SS	**70**	**3.3**	**4,800**
SS	**56**	**3.2**	**5,200**
SS	**56**	**3.8**	**3,200**
SS	**average value**	**3.3**	**4,950**
Cu	84	3.0	6,300
Cu	84	2.9	6,900
Cu	70	2.9	6,900
Cu	70	2.7	8,500
Cu	70	2.8	7,600
Cu	56	2.8	7,600
Cu	56	2.7	8,500
Cu	average value	2.8	7,470

Copper Droplets Substrate	Current (A)	Primary Dendrite Arm Spacing *XI*(in urn)	Calculated Cooling Rate (°C/sec.)
SS	53	3.8	7,700
SS	46	4.6	3,800
SS	46	5.0	2,800
SS	46	3.8	7,700
SS	39	4.1	5,800
SS	39	4.4	4,500
SS	average value	4.3	5,380
Cu	53	3.4	11,800
Cu	53	4.6	3,800
Cu	46	3.3	13,200
Cu	46	3.7	8,500
Cu	39	3.1	17,000
Cu	39	3.7	8,500
Cu	average value	3.6	10,470

The quality of the samples varied widely between samples, making it difficult to locate dendrite segments where consecutive arms could be counted. These results are measured from dendrites located close to the droplet centerline, and near the interface. There is considerable variability to the calculated cooling rates, with little apparent relation between the plasma current setting (i.e. the initial temperature of the droplet) and the cooling rate. The weakness of a relation is attributed to several factors: the importance of the location of the measurement, since the cooling rate at the interface will be greater than at the top surface of the droplet; and the variability of droplet temperature with the microcasting process, even under constant plasma power conditions.

Average cooling rate values for each subset of experiments more clearly show the relation between cooling rates and the materials involved. The highest cooling rates are experienced when copper substrates are involved (7,470°C/sec. for stainless steel droplets and 10,470°C/sec. for copper droplets), the lowest rates when stainless steel substrates are present (4,950°C/sec. for stainless steel droplets and 5,380°C/sec. for copper droplets). When considering the same substrate materials, copper droplets undergo slightly more rapid cooling than the stainless steel droplets, although the influence of droplet material is weaker than that of the substrate material.

Significant variation is present in the previous dendrite spacing analysis, with considerable overlap for cooling rate values between the different samples and application parameters. Therefore, a more accurate attempt was made at clarifying the relation between arm spacing (cooling rates) and initial droplet temperature, as well as the spatial variation of cooling rate values within individual droplets/substrates. For this next analysis, we use droplet samples generated by the maximum and minimum plasma power settings, and we measure dendrite arm spacing at consistent droplet locations within each sample.

Table 2 summarizes the droplet dendrite arm spacing results (measured in *\im)* for the eight samples investigated and an average value for each case. The top half of the table shows secondary dendrite spacing for the four cases with stainless steel droplets; the maximum plasma current is 84A, the minimum is 56A (temperatures at impact of 2,500°C and 2,000°C respectively). The stainless steel substrates are presented in the left columns, the copper substrates are to the right. Locations 1 through 4 represent approximately equal vertical spacing along the droplet centerline from the interface to the top of the droplet.

Locations l_v 5_9 6,7 are equally spaced along the interface from the centerline to the lateral edge of the droplet (see Figure 2). The lower data group in Table 2 is the copper droplet results, using primary dendrite spacing. The maximum plasma current setting for copper is 53A, and the minimum 39A (impact temperatures of 2,000°C and l,800°C, respectively).

Table 2. Dendrite Arm Spacing - Spatial Evaluation within Droplet

St. Steel on St. Steel

Location	56A	**84A**
	(in|im)	**(inum)**
1	**1.13**	1.00
2	**2.78**	**2.82**
3	3.05	3.42
4	3.27	2.17
5	2.59	2.72
6	2.63	1.95
7	1.29	2.00
average	2.39	2.29

St. Steel on Copper

56A	**84A**
(in urn)	**(inum)**
1.67	**n/a**
3.00	**2.27**
3.07	**2.63**
2.65	2.11
2.20	4.44
2.10	**5.0**
2.27	**3.29**
2.42	3.29

Copper on St. Steel

Location	39A	**53A**
	(inn-m)	**(in urn)**
1	**6.0**	**4.25**
2	7.14	7.33
3	6.0	5.6
4	3.0	4.0
5	4.75	6.4
6	4.57	5.14
7	4.86	3.8
average	**5.19**	**5.22**

Copper on Copper

39A	**53A**
(in|xm)	**(in tun)**
5.36	**n/a**
6.20	**6.20**
6.67	4.60
5.40	2.50
4.19	3.00
2.33	8.00
2.80	2.17
4.71	4.41

Gathering dendrite spacing results at consistent locations was again difficult to achieve. Some of the droplet samples did not show regular dendrite structure in the region we were seeking to characterize. However, as the sample location considered moves from the interface towards the top surface of the droplet, the dendrite spacing values show an increasing trend in most of the samples, indicating a decreasing cooling rate. There are exceptions to this trend though. The validity of these results would be enhanced if the same dendrite could be followed across the entire droplet, but this was rarely possible. Near the droplet surface, undercooling and nucleation from foreign material (copper in

stainless steel droplets and vice versa) can give rise to equiaxed structures that yield different dendrite spacing relations. The most consistent results are found with stainless steel droplets, particularly with stainless steel substrates. This combination avoids the difficulties caused by dissimilar material nucleation.

While a trend appears in the vertical direction, the results in the lateral direction show an absence of a strong spatial trend for the magnitude of the dendrite spacing between the centerline and the edge of the droplet. Spacing values for the edge locations along the interface are not significantly different from the centerline values. This is attributed to consistent cooling conditions across the droplet/substrate interface during the initial solidification of the droplet. It should be stressed that dendrite measurements near the interface are the most difficult to perform, particularly with the copper droplets, due to effects of fluid turbulence and chill zone structures at the substrate interface.

The last row for each of the samples is the averaged value of arm spacing for each case. This average value provides a basis for comparing the cooling rates at the different plasma power settings. It was expected that the higher temperature droplets (greater plasma current) would exhibit the higher cooling rates (smaller arm spacing). The samples of stainless steel on stainless steel, and copper on copper, show this trend to a slight extent. The stainless steel droplet on copper shows the reverse effect, and the copper droplet on stainless steel shows very little difference between the two plasma current setting extremes.

The last investigation using dendrite spacing correlations considered the cooling within the substrate region, particularly in the region where remelting takes place. Table 3 shows the dendrite arm spacing results for four substrate samples. The stainless steel droplets are the two left cases, the copper droplets are the two at the right. Three locations were selected in the substrate near the droplet interface: close to the droplet centerline, midway between the centerline and droplet edge, and near the droplet edge. These dendrite spacing results are in agreement with the lateral spacing results within the droplet region along the interface. No significant spatial trend is seen for the dendrite spacing along the interface.

Table 3. Dendrite Arm Spacing — within Substrate

Location	SS droplet SS substrate	SS droplet Cu substrate	Cu droplet Cu substrate	Cu droplet SS substrate
	(in|xm)	(in |i.m)	(in Mm)	(in |im)
center	3.33	3.08	5.63	4.08
middle	2.67	4.00	6.66	3.63
edge	3.63	4.67	3.60	3.33

The final goal of the microstructural characterization is to verify and quantify substrate remelting. Remelting is necessary for the creation of complete bonding between each layer of the microcasting artifact. A properly bonded artifact will have material properties and strength comparable with traditionally manufactured objects. We seek to ensure remelting across the entire droplet/substrate interface, but to avoid excessive bonding. Remelt bonding penetrating the substrate too deeply creates a loss of geometric tolerance and undesirable surface finish when dissimilar material interfaces are involved, indicates excessive heat to be dissipated, and results in the creation of unwanted thermal residual stresses.

The microstructure shown in Figure 4 at SOX magnification is for a stainless steel droplet with a 2,500°C temperature on impact, striking a stainless steel substrate that is initially at ambient temperature. The microstructure indicates a clear remelting line that is greatest near the centerline. At the edges of the droplet, the droplet energy is insufficient to achieve substrate remelting. By superimposing a straight line across the substrate interface, connecting the two clean interface lines at the edges of the droplet, the remelting taking place along the droplet can be measured. For this case, a maximum remelt depth that approaches 200 (im is measured. The microstructures of both the droplet and the substrate contain dark regions of chromium-rich delta-ferrite and light regions of nickel-rich austenite. The dark line that marks the deepest penetration of the remelted region results from an accumulation of chromium in the delta-ferrite phase at the front of the advancing remelting line. This remelting depth estimated by metallography compares well with the depths predicted by our numerical models.

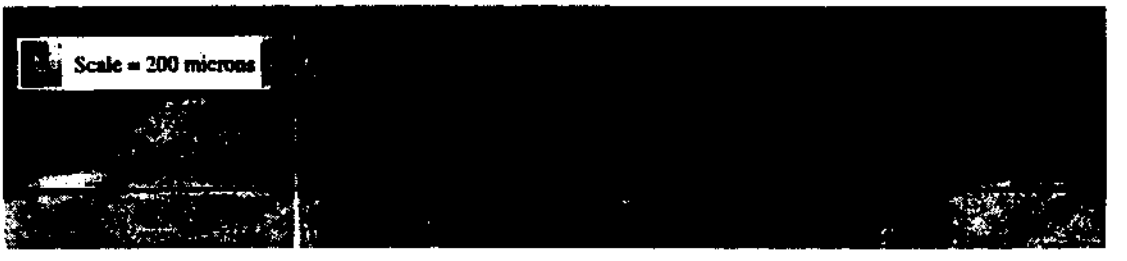

Figure 4. SOX magnification of stainless steel droplet on stainless steel substrate

Additional evidence that the dark line truly delineates remelting is found by examining the line of maximum remelting under a higher magnification. Figure 5 shows the remelt line for the same sample at a magnification of 1000X. The left picture, taken towards the center

of the droplet, reveals a continuation of the dendrite structure across the remelt line. This indicates that nucleation for the dendrites, when the remelted substrate begins to resolidify, is initiated from the existing dendrite structure in the substrate. Because this location is below the original substrate surface, remelting has taken place. The slight discontinuity of the dendrite angle across the remelt line is due to the difference in preferred growth direction of the different deposits. The right picture, taken near the edge of the droplet, does not possess this same continuity. This indicates that remelting has not taken place at the outer edge of the droplet.

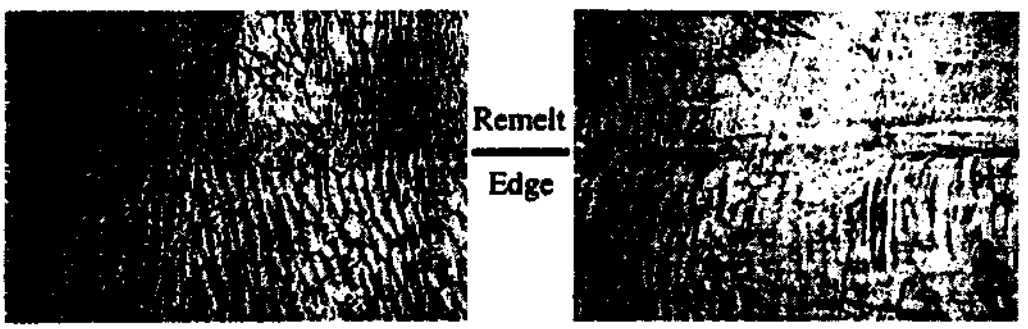

Figure 5. 1000X magnification of the remelt interface for a stainless steel droplet on a stainless steel substrate

The evaluation of remelting for a dissimilar material sample (either a stainless steel droplet on a copper substrate, or copper on stainless steel) is less straightforward than the previous case. Figure 6 shows a 50X magnification of the microstructure of a copper droplet on a stainless steel substrate, again with a superimposed line across the original surface of the substrate. While the interface between the two materials is clear, and there appears to be some degree of remelt bonding, the exact location of a remelted zone is more difficult to determine. We have two types of evidence of remelt bonding in these cases: (1) closer examination of the droplet region immediately adjacent to the interface shows the presence of dissimilar precipitate material within the droplet; and (2) distortions to the shape of the substrate interface are seen that can only be created by first melting the interface.

Figure 6. SOX magnification of copper droplet on stainless steel substrate

At a magnification of 1000X, the left side photograph in Figure 7 shows the interface rcgion between the copper droplet and the stainless steel substrate. There are small, dark precipitates within the copper region that appear to be stainless steel, and would have been convected into the copper during the initial spreading of the droplet across the substrate. In order to verify that these regions are stainless steel, we perform an energy dispersive X-ray analysis to characterize the small regions of dissimilar material (precipitates) observed in the copper. Figure 8 shows the results from this analysis.[1] The energy spectrum exhibited by the predominant, lighter droplet region is shown at the left to be copper, while the spectrum of the dark precipitate, seen at the right of Figure 8, verifies that the material is stainless steel. Cases where stainless steel droplets are deposited on copper substrates exhibit a similar formation of small, copper precipitates near the interface. In other examples, we have found stainless steel precipitates located in the upper regions of the copper droplet.

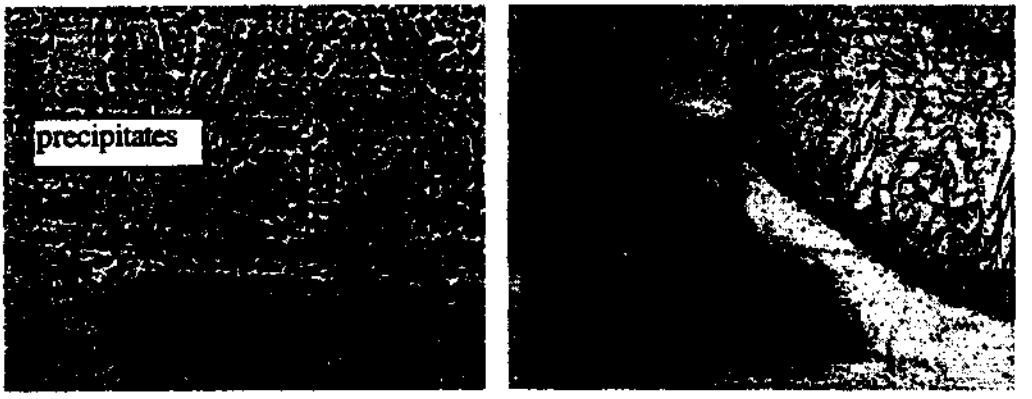

Figure 7. 1000X magnification pictures of copper/stainless steel interface

[1] **Performed by D. Kolluru at CMU.**

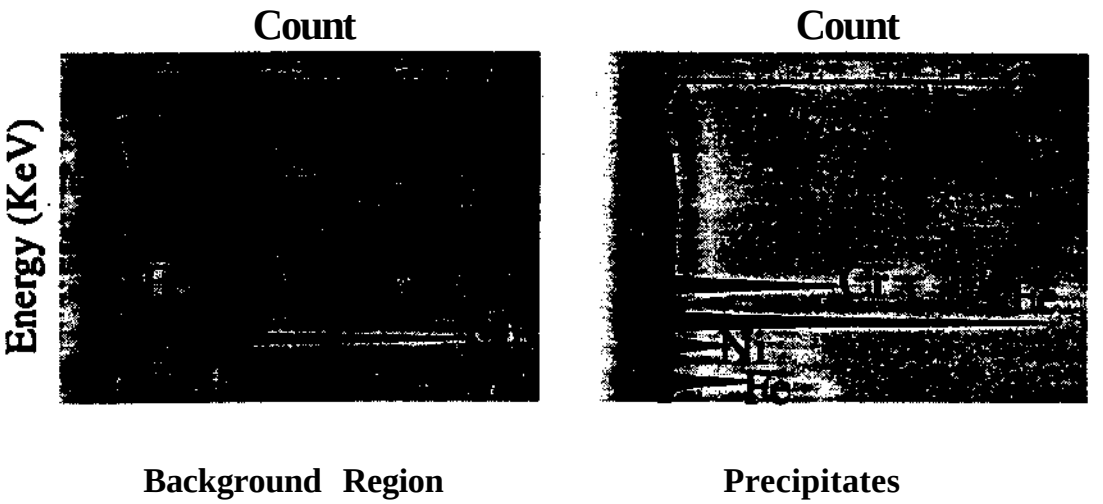

Figure 8. Energy spectrum from EDX analysis

The right side picture in Figure 7 shows another 1000X image of the copper droplet interface with a stainless steel substrate. In this case, the original stainless steel interface, which is milled flat prior to the deposition of the copper, is severely distorted. A portion of the stainless steel has even broken free from the lower substrate. This type of interface is evidence of the partial remelting of the stainless steel during deposition, since this could only be formed by first melting the stainless steel substrate.

Discussion and Summary:

The droplet microstructures formed during SDM microcasting are irregular and difficult to accurately characterize. The droplets undergo high cooling rates which yield fine microstructures and are subject to significant convective forces due to the motion of the impinging droplets which disrupt the growth patterns. Nonetheless, it is possible to gather useful information about the thermal behavior of the droplets by investigating the microstructure. The stainless steel droplets (either on stainless steel or copper substrates) exhibit the most consistent columnar microstructure. This indicates crystal growth constrained by heat removal. In addition, the orientation of the resulting structure clearly indicates that the heat removal is accomplished by conduction into the substrate (Honeycombe, 1981). The stainless steel droplet region closest to the substrate exhibits the least columnar structure, due to both the competitive growth directions of the initial crystal formation and also the bulk mixing of the liquid during the droplet's spreading, recoiling and oscillating prior to complete solidification. Slightly higher into the droplet (less than a

quarter of the total droplet height) a regular columnar dendrite pattern allows measurement of secondary dendrite spacing and comparison with correlations for cooling rates. The measurements yield an estimated droplet cooling rate of 5,000°C/sec. for the droplet striking a stainless steel substrate, and 7,500°C/sec. for a copper substrate. These results are expected, due to the significantly higher thermal conductivity of copper (350 W/m°Q as compared to stainless steel (25 W/m°C).

The copper droplet microstructure is less homogeneous than the stainless steel. While regions of columnar grain structure exist, predominantly along the droplet mid-height, there is a lack of structure similar to that seen with the stainless steel droplet cases closest to the interface of the substrate (due to fluid motion and initial competitive growth). The microstructure becomes more equiaxed as the upper surface is approached, particularly for droplets deposited on stainless steel substrates. Numerous pores or gas bubbles exist in the copper droplets, perhaps from absorption of the nitrogen shield gas by the liquid copper droplets, and evolution of the nitrogen during solidification. The equiaxed structure in the upper portion of the droplet indicates copper undercooling. A regular columnar microstructure in copper is further disrupted by the presence of stainless steel precipitates carried from the substrate into the droplet region. These stainless steel precipitates solidify before the copper (with a solidification temperature 400°C above copper) then act as nucleation sites during the solidification of the copper. Primary dendrite spacing measurements together with cooling rates correlations yield an estimated droplet cooling rate of 5,400°C/sec. for the stainless steel substrate case, and 10,500°C/sec. for a copper substrate. This again is indicative of the relative thermal conductivity values.

Prior to performing the experiments, we expected to find a finer dendrite structure near the substrate than at the surface, indicating greater cooling rates. We have identified a dependence between vertical spatial location within the droplet and the cooling rate experienced. The region closer to the interface experiences a greater cooling rate, which is to be expected given the greater temperature gradient early in the cooling process, and the increased resistance to heat flux imposed by the larger distances needed to conduct the heat into the substrate. Relations were not found between cooling rates and the lateral location across the interface, either within the droplet or substrate regions. The lack of any lateral effects results from the similarity of cooling conditions at the initial stages of cooling, which are due to the smaller time scales of droplet spreading as compared to solidification.

We have previously noted a multi-dimensional characteristic to the substrate heat transfer with microcasting (Amon et al$_M$ 1996a), but for the locations considered which lie in close proximity to the interface, the consistent dendrite spacing values reflect the one-dimensional nature of the droplet heat flux. The lack of a trend may also be attributed to the error or uncertainty in the correlations and measurements at the high cooling rates, the inability to accurately distinguish spacings at this scale, and the disruption to the growth patterns due to both bulk convective motions and the presence of foreign material (i.e. stainless steel in the copper droplet) acting as nucleating sites.

We did expect to find a discernible effect on the cooling rate arising from changes in the initial droplet temperature, particularly when the initial droplet temperatures change by several hundred degrees. A higher rate of cooling was expected for the hotter droplets, due to the larger thermal gradients. The absence of this trend is an indication of the variability of the temperature of the droplets created by the SDM microcasting process. The plasma torch provides a highly turbulent flow that may cause the melting droplets to fall from the feedwire in a non-uniform fashion. With the tremendous heat involved in the plasma arc, this may significantly alter the temperature of successive droplets, even under the same process conditions.

While the accuracy of the qualitative information gathered from the microstructural characterization may be limited, valuable qualitative insights about solidification are possible. The grain direction in the droplet region indicates the predominantly uni-directional nature of conduction heat transfer at the droplet/substrate interface. The solidifying material microstructure, which aligns in the preferred grain direction most nearly perpendicular to the isotherms, shows a distinct grain direction which is roughly perpendicular to the substrate surface. The directional solidification growth (columnar), instead of equiaxed, indicates the lack of undercooling for all of the cases except for copper droplets on stainless steel.

The microstructural characterization is able to address the issue of bonding between droplets and substrate. In all of the samples studied, the final interface between the droplet and substrate is not regular. Remelting of the substrate below the interface occurs, particularly near the droplet centerlines, although decreasingly towards the edges. For this study, individual droplets were purposefully deposited on a substrate at ambient temperature. Compared to regular microcasting, where a series of adjacent droplets are deposited and heat the entire substrate, these conditions are less conducive for remelting.

Complete remelting during regular SDM microcasting is therefore expected across the entire droplet interface.

The most straightforward measurement of substrate remelting is possible with the stainless steel droplet on a stainless steel substrate (Figure 4). For this case a maximum remelting of 200 |im exists, although complete remelting across the entire droplet interface is not achieved. The copper on copper cases were more difficult to interpret, because the copper substrate previously deposited was very thin, and the impinging copper droplet seemed to melt the entire substrate layer. For the dissimilar material cases, remelting was verified by virtue of the incorporation of substrate material into the droplet region. There are also clear examples along the substrate where the original surface is distorted to a degree only possible if the substrate had become molten (Figure 7b). Material characterization by EDX has been used to positively identify the material present. The extent of remelting for these dissimilar material cases cannot be verified. An additional test that we are planning to perform is apply EDX identification vertically across the interface, and by locating the region with a mixture of materials, we will be able to estimate the remelted zone.

Acknowledgments:

Our analysis of the microstructure results was greatly assisted by supporting work performed by Dakshinamurthy V. Kolluru and by comments from Dr. Alan Cramb.

Financial support by the Advanced Research Project Agency, Contract DABT63-95-C-0026, Engineering Design Research Center grant EDC-8943164, and National Science Foundation Grants DMI-9415001 and CTS-9630801 is gratefully acknowledged.

Bibliography:

Amon, C.H., Schmaltz, K.S. Merz, R. and Prinz, F.B., 1996a, "Numerical and Experimental Investigation of Interface Bonding Via Substrate Remelting of an Impinging Molten Metal Droplet," *ASME J. of Heat Transfer*, Vol. 118, pp. 164-172,

Amon, C.H., Beuth, J.L., Merz, R., Prinz, F.B. and Weiss, L.E., 1996b, "Shape Deposition Manufacturing with Microcasting: Processing, Thermal and Mechanical Issues," *ASME J. Manufacturing Sciences and Engineering*, under review.

Honeycombe, R.W.K., 1981, *Steels Microstructure and Properties*, The Macmillan Co., London.

Merz, R., 1994, "Shape Deposition Manufacturing," Ph.D. Thesis, Department of Electrical Engineering, Technical University of Vienna, Austria.

Mills, K., *et at*, ed., 1985, *Metals Handbook, Metallography and Microstructures*, Vol. 9 American Society for Metals, Metals Park, OH, pp. 637-640.

Osio, I.G. and Amon, C.H., 1996, "An Engineering Design Methodology with Bayesian Surrogates and Optimal Sampling," *Research in Engineering Design*, Vol. 8, No. 4, pp. 189-206.

Osio, I.G., 1996, "Multistage Bayesian Surrogates and Optimal Sampling for Engineering Design and Process Improvement," Ph.D. Thesis, Department of Mechanical Engineering, Carnegie Mellon University, Pittsburgh, PA.

Osio, I.G., Padmanabhan, P., Amon, C.H. and Finger S., "Combining Experimental and Statistical Methods for Quality Improvement of Microcasting Shape Deposition Manufacturing," *Manufacturing Science and Engineering*, submitted 1997.

Padmanabhan, P., 1996, "Process Planning for Quality: Shape Deposition Manufacturing," Ph.D. Thesis, Department of Mechanical Engineering, Carnegie Mellon Univ., Pittsburgh, PA.

Wolf, M., 1986, "Strand Surface Quality of Austenitic Stainless Steels: Part 2 Microscopic Solidification Structure," *Ironmaking and Steelmaking*, Vol. 13, No. 5, pp. 258-262.